Colloquium: Emergent properties in plane view: Strong correlations at oxide interfaces

Jak Chakhalian

Department of Physics, University of Arkansas, Fayetteville, Arkansas 72701, USA

John W. Freeland

Advanced Photon Source, Argonne National Laboratory, Argonne, Illinois 60439, USA

Andrew J. Millis

Department of Physics, Columbia University, 538 West 120th Street, New York, New York 10027, USA

Christos Panagopoulos

School of Physical and Mathematical Sciences, Division of Physics and Applied Physics, Nanyang Technological University, 637371 Singapore

James M. Rondinelli*

Department of Materials Science and Engineering, Drexel University, Philadelphia, Pennsylvania 19104, USA

(published 13 October 2014)

Finding new collective electronic states in materials is one of the fundamental goals of condensed matter physics. Atomic-scale superlattices formed from transition metal oxides are a particularly appealing hunting ground for new physics. In bulk form, transition metal oxides exhibit a remarkable range of magnetic, superconducting, and multiferroic phases that are of great scientific interest and are potentially capable of providing innovative energy, security, electronics, and medical technology platforms. In superlattices new states may emerge at the interfaces where dissimilar materials meet. This Colloquium illustrates the essential features that make transition metal oxide-based heterostructures an appealing discovery platform for emergent properties with a few selected examples, showing how charge redistributes, magnetism and orbital polarization arises, and ferroelectric order emerges from heterostructures comprised of oxide components with nominally contradictory behavior with the aim providing insight into the creation and control of novel behavior at oxide interfaces by suitable mechanical, electrical, or optical boundary conditions and excitations.

DOI: 10.1103/RevModPhys.86.1189 PACS numbers: 71.27.+a

CONTENTS

I. INTRODUCTION

Finding new collective electronic states in materials is one of the fundamental goals of condensed matter physics. While the traditional approach has been to search for such phases within naturally occurring compounds, in recent years the focus has shifted to *heterostructures* (Hwang *et al.*, 2012): artificial materials formed by interleaving two or more structurally and chemically dissimilar materials. Of particular interest is the spatial region at the *interface* where dissimilar

*Present address: Department of Materials Science and Engineering, Northwestern University, Evanston, Illinois 60208, USA.

materials meet. New states may emerge here because the environment near an interface is different from that occurring in bulk (thermodynamically stable) materials. Advances in the *angstrom-scale* layer-by-layer synthesis of multielement compounds for *materials by design* have taken the approach to a new level of power and sophistication: It enables the atomic-scale combination of materials with different properties, granting access to a new terrain in which unusual states of matter may arise (Schlom *et al.*, 2008).

Heterostructures formed from transition metal oxides (TMO) are a particularly appealing hunting ground for new physics. In these materials the transition metal (M) ion has an open d-shell electronic configuration with spin, orbital, and charge degrees of freedom. Electrons in these partially filled d shells are *correlated*: The motion of one electron depends explicitly and nontrivially on the behavior of all of the others giving rise to interesting many-body phenomena (Imada, Fujimori, and Tokura, 1998). The resulting magnetic, superconducting, and multiferroic phases are of great scientific interest and are potentially capable of providing innovative energy, security, electronics, and medical technology platforms. The heterostructure geometry (Mannhart and Schlom, 2010; Zubko *et al.*, 2011; Granozio, Koster, and Rijnders, 2013) enables otherwise unattainable changes in atomic structure and chemical bonding, leading to new modalities for control and optimization of known states and potentially leading to new ones.

Over the past decade, one particular class of heterostructures, based on the interface between lanthanum aluminate [$LaAlO_3$ (LAO)] and strontium titanate [$SrTiO_3$ (STO)], has been the subject of very extensive study. In this Colloquium we choose not to discuss the LAO and STO interface or its variants, selecting our examples instead from vanadate, manganite, cuprate, and nickelate-based systems for two reasons. First, the LAO and STO system and its variants have been extensively reviewed in other venues; see, for example, Mannhart *et al.* (2008), Hwang *et al.* (2012), and Zubko *et al.* (2011). Second, and more importantly, the LAO and STO system involves doping nominally insulating STO with maximum sheet carrier densities of fewer than 0.5 electrons (e) per in-plane unit cell, and the charge density is typically spread over several unit cells in the direction perpendicular to the interface. The volume carrier densities are therefore typically low, so that the situation is more closely related to a doped semiconductor than to the correlated electron materials on which we wish to focus here. Nonetheless, some of the scientific excitement has focused on superconductivity (Reyren *et al.*, 2007) (exhibited also when bulk STO is lightly doped by conventional dopants) and Anderson localization metal-insulator transitions (MITs) (Caviglia *et al.*, 2008). Reports or theoretical suggestions of other correlation phenomena in this system including charge ordering (Pentcheva and Pickett, 2007) and magnetism (Okamoto, Millis, and Spaldin, 2006; Brinkman *et al.*, 2007; Ariando *et al.*, 2011; Bert *et al.*, 2011; Li *et al.*, 2011) have also appeared; we return to the issue in Sec. IV and in the Conclusions.

This Colloquium illustrates the essential features that make TMO-based heterostructures an appealing discovery platform for emergent properties. The guiding principle is that strong electronic correlations in combination with the access to new symmetries and electronic band structures provided by oxide interfaces can activate new electronic properties formerly "hidden" in bulk compounds. We illustrate this principle with a few selected examples, showing how charge redistributes, magnetism and orbital polarization arises, and ferroelectric order emerges from heterostructures comprised of oxide components with nominally contradictory behavior. For example, interfaces may be metallic, magnetic, or ferroelectric even though in bulk form the constituent materials are insulating, nonmagnetic, or simple dielectrics. We conclude by articulating open challenges and opportunities in the field, in particular, how to translate the new understanding of when emergent phases arise into control of novel behavior by design at oxide interfaces, and the manipulation of these states by suitable mechanical, electrical, or optical boundary conditions and excitations.

II. ANATOMY OF AN OXIDE INTERFACE

The formation of a coherent perovskite oxide heterointerface, as shown in Fig. 1, provides a remarkable correlated electron "playground." It brings different transition metal cations with their localized d electron physics and interacting charge, spin, and lattice degrees of freedom into intimate contact in a tunable crystalline environment.

The key structural features of transition metal oxides relate to the coordination geometry of the metal ions and the metal-oxygen–metal-bond angles. These determine magnetic exchange interactions (Anderson, 1950; Goodenough, 1955; Kanamori, 1959) and electronic bandwidths (Eng *et al.*, 2003), thereby controlling the electronic and magnetic ground states. Structural and electronic changes across an interface can act to stabilize previously unanticipated phases of matter (Okamoto and Millis, 2004).

Consider, for example, a multilayer heterostructure comprised of alternating blocks of the metallic ferromagnet $La_{2/3}Ca_{1/3}MnO_3$ (LCMO), and the high-temperature cuprate superconductor $YBa_2Cu_3O_{7-x}$ (YBCO) sketched in Fig. 1. The interface brings several crucial structural effects. The first is a coordination mismatch. LCMO is a three-dimensional perovskite (AMO_3 stoichiometry) with corner-connected MnO_6 octahedra that may be described by interleaving alternating (La,Ca)O and MnO_2 layers along [001]. In contrast, YBCO is a two-dimensional oxide with fourfold and fivefold coordinated Cu cations. The layered cuprate structure may be considered as a derivative of perovskite, which partly facilitates coherent growth of the heterostructure. But unlike LCMO, YBCO displays an ordered network of oxygen vacancies accommodated by the valence preferences of Cu: One oxygen atom is removed from every third (001) AO plane to produce the square pyramidal CuO_5 coordination, then on every third CuO_2 layer, vacancies order along [100], producing the square planar CuO_4 coordination. Thus a "coordination mismatch" arising from the change from the sixfold coordination of the Mn to the lower coordination of the Cu (Fig. 1, lower left) occurs at the interface. As a result, a set of CuO chains (i.e., charge reservoir) is missing from the interfacial YBCO unit cell to maintain a prerovskitelike

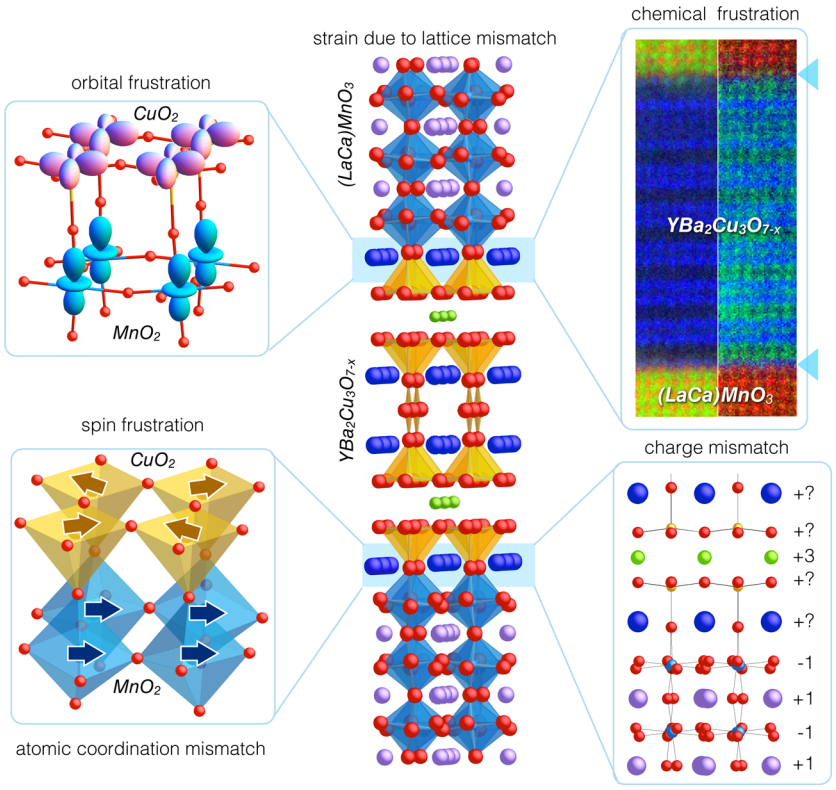

FIG. 1 (color online). Anatomy of an oxide heterointerface: an illustration showing the interplay between different degrees of freedom (charge, spin, and lattice) at a coherently grown interface between ferromagnetic $La_{2/3}Ca_{1/3}MnO_3$ and superconducting $YBa_2Cu_3O_{7-x}$. The electron micrograph is reproduced from Chien *et al.* (2013), where each color represents a different chemical species.

sequence $\cdots MnO_2 - BaO - CuO_2 \cdots$ across the junction (Zhang *et al.*, 2009; Chien *et al.*, 2013).

Coherent epitaxial growth also produces an intrinsic strain mismatch arising from the different equilibrium lattice constants (Fig. 1, center). The atomic structure at the heterointerface responds to alleviate the strain mismatch through relaxation of the interatomic distances and internal atomic degrees of freedom (for example, rotations or size deformations to the transition metal oxygen polyhedra) in the constituents along the superlattice repeat direction. These new atomic arrangements directly alter the electronic structure. Away from the interface it is characterized by carriers in the d manifold with orbital symmetries $d(x^2 - y^2)$ (YBCO) and $d(3z^2 - r^2/x^2 - y^2)$ for LCMO (Fig. 1, upper left), but near the interface the $d(3z^2 - r^2)$ become occupied in the YBCO and acquire more $d(x^2 - y^2)$ character in the LCMO.

In addition to the structural effects, an electronic mismatch occurs. The ferromagnetism in LCMO relies on the cooperative *parallel* alignment of spins from the narrow correlated electronic bands; singlet Cooper pair formation in YBCO, in contrast, relies on *paired* spins with antiferromagnetic (AFM) interactions. These antagonistic spin interactions (frustration) have been invoked to explain changes in the interfacial magnetization and superconductivity, e.g., giant magnetoresistance, the appearance of an uncompensated magnetic moment on Cu in the CuO_2 plane, and a large modulation of the ferromagnetic (FM) magnetization profile across the heterojunction (Peña *et al.*, 2005; Stahn *et al.*, 2005; Chakhalian *et al.*, 2006; Hoppler *et al.*, 2009)

The different valence configurations of the cations in the constituent materials of the heterostructure also induce changes in charge density and chemical bonding. In the system shown in Fig. 1 (lower right panel) a charge of $\sim 0.2e$ per Cu ion is transferred from Mn to Cu ions across the interface (Chakhalian *et al.*, 2007). The charge transfer at other oxide interfaces has also been found to exhibit a peculiar asymmetric electronic "roughness" intertwined with an asymmetric interface stacking sequence or an asymmetric chemical roughness (Hoffmann *et al.*, 2005; May *et al.*, 2008; Chien *et al.*, 2013). The effects from different stacking sequences and electronic roughness remain to be resolved.

To summarize, the following degrees of freedom are highly tunable at an oxide interface and may be exploited in uncovering new phases:

- epitaxial strain mismatch owing to differences in equilibrium lattice parameters,
- atomic coordination frustration and cation site preferences,
- ordered spin and orbital states,
- charge flow across the interface (layer dipole discontinuities),
- chemical frustration and interlayer mixing, and
- competing phases placed in close proximity.

The following examples detail how these considerations are made and the exciting new phases born from the interplay of the correlated electronic and atomic structure across oxide interfaces.

III. CHARGE AT THE INTERFACE

Understanding and controlling the distribution of charge carriers at the interface between dissimilar semiconductors is one of the pivotal developments of modern microelectronics (Gertner, 2013), important both for devices and as a crucial platform for discovery of remarkable physical phenomena including integer and fractionally quantized Hall effects as well as spin-Hall and other spintronic phenomena.

In conventional semiconductor heterojunctions the basic physics is driven by the difference in work function, which causes charge transfer across the boundary to equalize chemical potentials. The work-function difference may be manipulated by a process known as δ doping (Schubert, 1990; Harris *et al.*, 1991), in which a layer of ions is implanted in a plane at some distance from the interface. An additional advantage of δ doping is that the placement of the dopants at some distance from the interface minimizes the effects of randomness in the dopant positions. δ doping is now widely used to produce two-dimensional electron gases (2DEGs) confined to the proximity to the interface (e.g., GaAs/AlGaAs).

The interest in using TMO to explore similar physics was motivated by two observations (Ahn, Triscone, and Mannhart, 2003; Ahn *et al.*, 2006): (i) in oxides, the accessible carrier density is expected to be orders of magnitude higher than that of semiconductors ($\geq 10^{20}$ cm^{-3}); and (ii) the Thomas-Fermi screening length is expected to be much shorter, so the charges may be confined to within $<$ 1–2 nm of the interface, a factor of 5–10 shorter than the ~10 nm length characteristic of semiconductor junctions. However, the current intense effort in material synthesis, theory, and device fabrication of oxide interfaces is motivated mainly by the known sensitivity of the correlated electron properties of transition metal oxides to the *d*-band filling (Tokura and Tomioka, 1999; Dagotto, Hotta, and Moreo, 2001; Mackenzie, 2003; Ovchinnikov, 2003; Basov, 2005; Lee and Wen, 2006; Tokura, 2006; Armitage, Fournier, and Greene, 2010). The discovery of an interface-based method of carrier doping has revived the idea of tailoring the materials electronic properties and creating novel quantum states not easily attainable in the bulk counterparts. The basic idea (analogous to that motivating δ doping) is to explore electronic and magnetic phases without the hindering effects of chemical disorder inherent in the conventional solid-state chemistry methods of changing carrier concentration.

During the past several years, extensive experimentation has established the fact that perovskite-based heterostructures are particularly susceptible to interlayer charge redistribution derived from the incompatibilities illustrated in Fig. 1 making them ideal candidates to explore such possibilities (Ohtomo *et al.*, 2002; Ohtomo and Hwang, 2004; Okamoto and Millis, 2004; May *et al.*, 2009; Bibes, Villegas, and Barthelemy, 2011).

A. Interface doping of a high-T_c superconductor

To illustrate the inherent interest of charge reconstruction on interfacial states, we discuss as one of many possible examples the recent progress on cuprate and manganite heterointerfaces. Macroscopically it has been established that the introduction of a ferromagnetic $(La, Ca)MnO_3$ manganite layer into the heterostructure with an optimally doped YBCO cuprate triggers a *suppression* of the superconducting transition temperature accompanied by a reduced ferromagnetic Curie temperature (Sefrioui *et al.*, 2003; Holden *et al.*, 2004; Peña *et al.*, 2004; Hoppler *et al.*, 2009; Kalcheim *et al.*, 2011; Driza *et al.*, 2012; Satapathy *et al.*, 2012). In a recent set of experiments (Fig. 2), *L*-edge polarized resonant x-ray absorption spectra taken at the Mn and Cu edges reveal the presence of a chemical shift implying a flow of electronic charge across the interface of about ~0.2*e* per Cu atom (Chakhalian *et al.*, 2007; Chien *et al.*, 2013). The depleted electrons from the MnO_2 layer are directly transferred to the CuO_2 planes, unbalancing the charge distribution between the atomic CuO_2 layers and the CuO chain charge reservoir block. The average Mn valence also increases from the as-grown value ($Mn^{+3.33}$) to around 3.5, indicative of covalent bond formation across the Mn–O–Cu interface.

The charge transfer across the interface from the Mn to Cu ions induces a major reconstruction of the *d*-orbital occupancies and frontier orbital symmetries in the interfacial CuO_2 layers (Chakhalian *et al.*, 2006, 2007). In particular, the Cu $d(3z^2 - r^2)$ orbital, which is fully occupied and electronically inactive in the bulk cuprates, becomes active at the interface

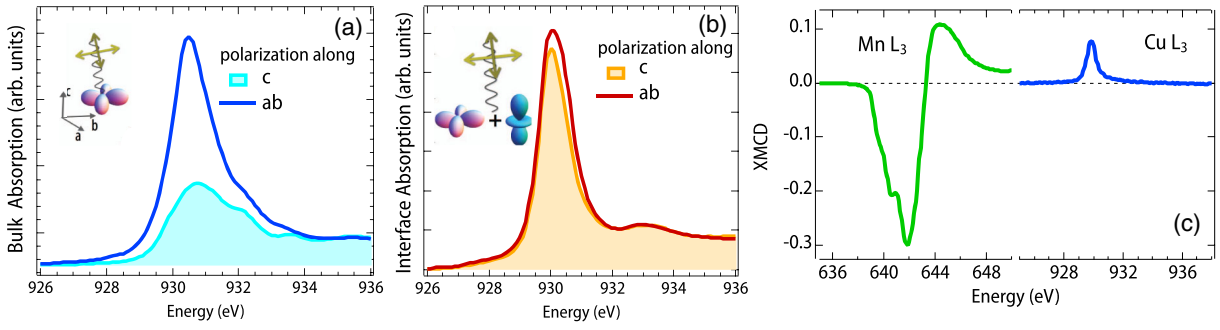

FIG. 2 (color online). Electronic structure of Cu in a $La_{2/3}Ca_{1/3}MnO_3/YBa_2Cu_3O_{7-x}$ heterostructure, determined from x-ray linear dichroism (XLD) and x-ray magnetic circular dichroism (XMCD) measurements. XLD spectra taken on the Cu L_3 edge at temperature $T = 15$ K with the electric-field vector $E\|ab$ plane and $E\|c$ plane, taken in (a) bulk and (b) interface sensitive modes. The main peak ("white line") in (b) is shifted toward higher energies, indicating a lower charge state of Cu at the interface. XMCD spectra measured at the Cu and Mn L_3 edges in (c) recorded at $T = 15$ K in a 5 T applied magnetic field demonstrating that the interfacial copper cations exhibit a nonzero ferromagnetic local moment, whereas in bulk the antiferromagnetic coupling leads to a net magnetization of zero.

[Fig. 2(b)]. At the same time charge transfer is observed in the presence of enhanced covalent chemical bonding across the interface, the Cu cations from the nominally antiferromagnetic CuO_2 plane acquire an uncompensated magnetic moment [Fig. 2(c)], attributed to spin canting of the local moments on the interfacial Cu cations.

Initial studies of the interplay between the ferromagnetic and superconducting order parameters used synchrotron based x-ray and neutron reflectivity experiments. However, these tools were unable to clearly resolve the length scale of interactions at the boundary between the two phases. Very recently, the issue was addressed by use of cross-sectional scanning tunneling microscopy (XSTM) together with atomic-resolution electron microscopy [scanning transmission electron microscopy (STEM) with electron energy loss spectroscopy (EELS)]. These methods enable direct observation of the charge distribution and the corresponding spatial scale for the buried interface (Chien *et al.*, 2013). Figure 3 shows the spatially resolved dI/dV spectra, which provided the first direct evidence that the length scale for charge transfer between YBCO and LCMO has an upper limit of < 1 nm, and that the spatial broadening of the electronic transition is commensurate with the rougher interface. This result sets a fundamental upper limit on the charge-transfer length scale in the YBCO and LCMO system, ruling out a class of theories based on long-range proximity effects (Hoffmann *et al.*, 2005). In addition to the established x-ray and neutron based probes, this powerful characterization technique provides a useful tool to achieve a microscopic direct space understanding of the electronic structure across correlated oxide interfaces.

B. Additional considerations

The complex behavior occurring at the LCMO and YBCO interface highlights the need to develop a clear language and set of concepts to describe interface electronic physics in correlated oxides. The inherently many-body nature of the correlated interface raises fundamental questions, in particular, of the applicability of the ideas, formulas, and language devised for semiconductor interfaces where a single-particle description works well. Pioneering work of Oka and Nagaosa (2005) showed via density matrix renormalization group calculations of a one-dimensional model system (in essence the one-dimensional Hubbard model with a spatially varying interaction parameter and band bottom) that the standard concepts of band bending and interface dipole apply, albeit with some modifications, as long as the conduction and valence bands are replaced by lower and upper Hubbard bands.

A growing body of literature builds on this work, using the concepts of band bending, Schottky barriers, and depletion layer creation borrowed from semiconductor physics (Hikita *et al.*, 2009; Yajima, Hikita, and Hwang, 2011), as well as more involved approaches, which unite Poisson-Schrödinger electrostatics with Mott-Hubbard physics (Okamoto and

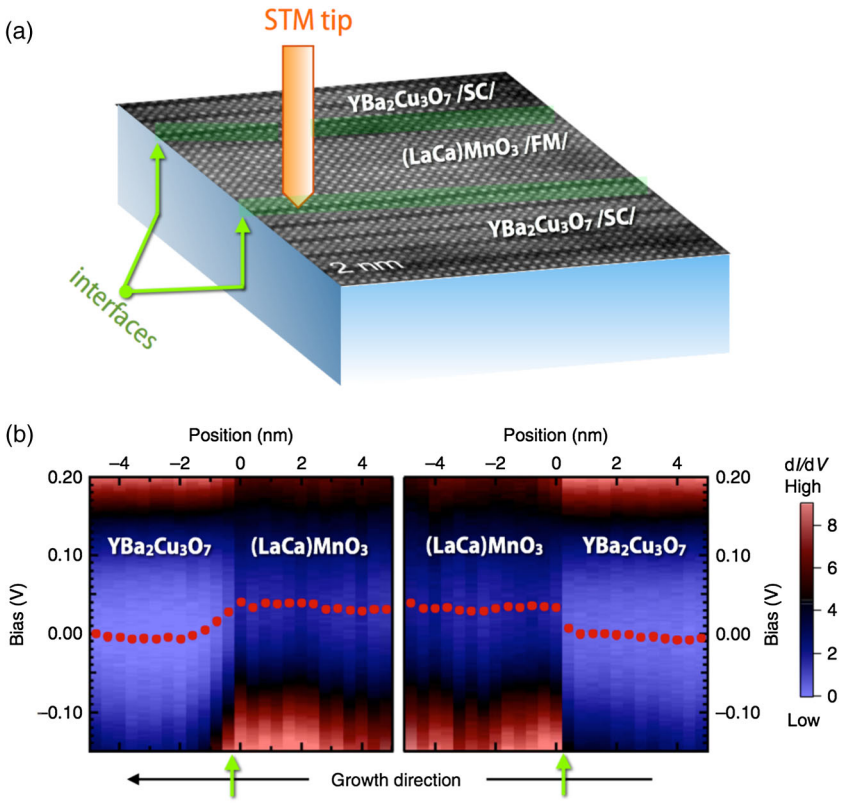

FIG. 3 (color online). (a) Schematic of cross-sectional scanning tunneling microscopy (XSTM) measurements performed on an LCMOand YBCO superlattice grown on a Nb-doped STO substrate. (b) The spatial evolution of the dI/dV spectra averaged across the two identically terminated heterointerfaces reveals that the electronic transition is more abrupt for the bottom interface (right arrow) than the top, broader, interface (left arrow). The dots represent the voltage of the minimum in the density of states. From Chien *et al.*, 2013.

Millis, 2004; Lee and Macdonald, 2006; Charlebois *et al.*, 2013). Correlation physics is shown to lead to quantitative changes in the spatial confinement of carriers near interfaces (Okamoto and Millis, 2004; Lee and Macdonald, 2006, 2007), including the possible formation of extended depletion regions of zero compressibility (so-called "Mott plateaus") (Lee and Macdonald, 2006; Charlebois *et al.*, 2013). Other theoretically proposed possibilities unattainable with semiconductor junctions include a spontaneously emerging quantum-well structure when an electron-doped Mott-Hubbard insulator is coupled to a normal metal with a large work function. Following the same line of reasoning, in a *p-n* junction between two correlated insulators the local Mott gap collapses giving rise to a 2DEG (Charlebois *et al.*, 2013).

With few exceptions (Jin *et al.*, 2011; Kareev *et al.*, 2013), current experimental attention has focused on interfaces such as those between the two band insulators $LaAlO_3$ and $SrTiO_3$. In most of these situations the carriers are introduced via the polar catastrophe mechanism (Mannhart *et al.*, 2008); the maximum sheet carrier density is 0.5 per in-plane unit cell and this carrier density is typically distributed (Okamoto, Millis, and Spaldin, 2006; Mannhart *et al.*, 2008) over several unit cells away from the interface, leading in general to volume carrier densities far below the Mott value of 1 per unit cell. Density functional plus Hubbard U calculations (Pentcheva and Pickett, 2007) indicate that a charge ordered phase in which the entire polar catastrophe charge density is in the first interface layer may be possible, but these suggestions have not yet been confirmed by experiment or beyond-DFT (density functional theory) methods. One very interesting potential exception is the work of Moetakef *et al.* (2012) on $GdTiO_3/SrTiO_3$ heterostructures, where a nontrivial insulating phase was observed when two layers of $SrTiO_3$ were sandwiched between thick sheets of $GdTiO_3$. It was explained by Chen, Lee, and Balents (2013) in terms of a novel "Mott dimer" phase, where the carrier density is far below the one electron per transition metal ion value needed for Mott physics; nonetheless many theoretical predictions suggest alternative avenues for emergent properties to arise and warrant experimental investigation.

Additional issues beyond conceptual approaches to interface control arise. The length scales in correlated oxides are typically very short, so the details of the interface may be more important than in conventional semiconductors. A local picture is needed, which is able to address the formation of chemical bonds across the junction, differing electronegativities of transition metal ions, changes in both crystal field energies and Madelung potentials, and polarity effects (Ohtomo and Hwang, 2004; Herranz *et al.*, 2007; Hotta, Susaki, and Hwang, 2007; Savoia *et al.*, 2009; Sing *et al.*, 2009; Takizawa *et al.*, 2009; Zhong, Xu, and Kelly, 2010; Biscaras *et al.*, 2012; Garcia-Barriocanal *et al.*, 2013; Park *et al.*, 2013; Salluzzo *et al.*, 2013).

A further complication is that while many correlated oxides are reasonably well described by the Mott-Hubbard picture on which the above-cited works are based, some important functional TMO are *charge-transfer* compounds (Zaanen, Sawatzky, and Allen, 1985; Khomskii and Sawatzky, 1997; Imada, Fujimori, and Tokura, 1998). The role of the lower Hubbard band in these materials is usurped by the ligand states (typically oxygen $2p$), thus implying a very different physical character for the doped holes (mainly in oxygen levels) and doped electrons (mainly in transition metal d levels). As a result, the alignment of the oxygen levels across the interface becomes crucial.

For all of the materials discussed in this Colloquium, theoretical treatments which go beyond the simple Hubbard model, including chemically realistic structures and energetics on the same footing as correlation effects, are needed, as are experimental investigations of systems with higher electron densities and complete control over cation and oxygen stoichiometry.

IV. CONTROL OF MAGNETISM WITH OXIDE HETEROSTRUCTURES

Long-range magnetic order in transition metal oxides usually arises from a combination of local moment formation on the transition metal site and intersite coupling via the oxygen sublattice. Heterostructures offer an opportunity to generate new magnetic states by manipulating both the moment formation and the nature of the intersite coupling. As examples, we note that the paramagnet $LaCoO_3$ can be converted to a FM material by tensile epitaxial strain, which changes the material from a low-spin to a high-spin state (Fuchs *et al.*, 2007; Freeland, Ma, and Shi, 2008; Park *et al.*, 2009; Rondinelli and Spaldin, 2009). On the other hand, bulk AFM $EuTiO_3$ can be converted to a ferromagnetic insulator under modest tensile strains (Lee *et al.*, 2010). Another notable example is the comprehensive study by Seo *et al.* (2010), which examined three-component $SrRuO_3$/manganite/$SrRuO_3$ heterostructures. They found strong compressive strain causes relative FM alignment of magnetization in the heterostructure layers, while tensile or weak compressive strain favors AFM alignment of neighboring layers.

This sort of control over local magnetization in thin film geometries is of potential utility for oxide electronics and spintronic applications, including magnetic memory and sensing (Bibes, Villegas, and Barthelemy, 2011). For example, electromechanical coupling via a piezoelectric material can be used to control the orientation and strength of the magnetization by tuning the lattice parameters of the heterostructure through an applied electric field (Dekker *et al.*, 2011). Here we focus on going beyond strain control to make use of the broken symmetry at the interface between two dissimilar materials to generate unique spatially structured magnetic states.

A. Creating novel magnetic states at interfaces

One approach to manipulating magnetism involves interfacial charge transfer in heterostructures created from an antiferromagnetic *insulator* and a paramagnetic *metal* (Takahashi, Kawasaki, and Tokura, 2001; Freeland *et al.*, 2010; Yordanov *et al.*, 2011). The choice of materials in this case was determined by two key factors: first, creating moments from a material without any propensity to moment formation, i.e., zero moments, is difficult. It is therefore reasonable to begin then by choosing a system with a large local moment such as $CaMnO_3$ with $3\mu_B$/Mn, which in bulk is

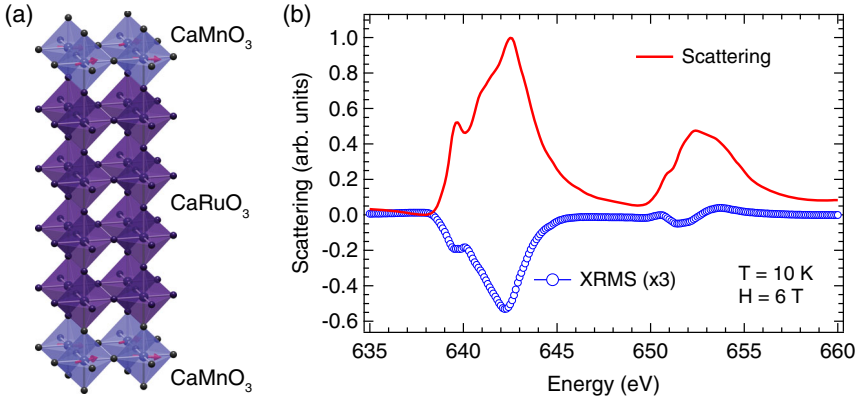

FIG. 4 (color online). (a) Schematic crystal structure showing canted spins (arrows) within the MnO_6 octahedra of $CaMnO_3$ at the interface of the quantum-well structure with metallic $CaRuO_3$. The canting arises from electron transfer owing to the Ohmic contact. (b) X-ray resonant magnetic scattering data showing a large magnetic signature arising from the FM alignment of spins at the interface in the presence of a magnetic field [see associated data in Freeland *et al.* (2010)].

a G-type (conventional two-sublattice Néel) antiferromagnet. However, modest electron doping of this material leads to strong FM correlations (Neumeier and Cohn, 2000). In a quantum-well heterostructure in which a paramagnetic metal (in this case $CaRuO_3$) is confined between two thick layers of $CaMnO_3$ one can expect that charge transfer from the metal to insulating $CaMnO_3$ will lead to interfacial doping and thus ferromagnetism.

Theoretical studies substantiate this argument and find that a charge of approximately $0.1e$ per interface unit cell leaks across the interface and is confined within ~1 unit cell at the $CaRuO_3/CaMnO_3$ interface (Nanda, Satpathy, and Springborg, 2007). Although the magnitude of the charge leakage is small, it has a significant impact on the antiferromagnetic order in the $CaMnO_3$, providing a mechanism for spin canting which yields large ferromagnetic moments at the interface (Takahashi, Kawasaki, and Tokura, 2001; Freeland *et al.*, 2010; Yordanov *et al.*, 2011). To validate this concept a study of the spatial distribution of the magnetism was carried out using x-ray resonant magnetic scattering (XRMS) at the Mn L edge (Freeland *et al.*, 2005; Kavich *et al.*, 2007). Figure 4 shows the large XRMS signal and that it deviates from the anticipated bulk G-type AFM state, which shows no ferromagnetic component to the magnetic moment under identical strain conditions indicating that the ferromagnetism emerges from the interface (Freeland *et al.*, 2010). By fitting this signal as a function of the incident angle, the extent of the magnetic polarization away from the interface was found to extend over several unit cells in contrast to the length of one unit cell predicted by theory (Nanda, Satpathy, and Springborg, 2007). The observed longer length scale of the magnetization profile discrepancy may be due to magnetic polarons, which are known to exist in lightly doped $CaMnO_3$ (Chiorescu, Cohn, and Neumeier, 2007), but such interfacial polarons have not been explicitly investigated theoretically.

B. Other routes to interface magnetism

Strain and layer sequencing can offer additional handles to manipulate the interfacial magnetic state in the $CaRuO_3/CaMnO_3$ system (He *et al.*, 2012). The link between the metallic layer and magnetism is best illustrated by studying superlattices, where the metallic layer undergoes a metal-to-insulator transition when the dimensionality is reduced in the ultrathin layer, and correspondingly the magnetism disappears (Grutter *et al.*, 2013). One can use this understanding and exploit it to design new functional materials and there are many possibilities that exist within the perovskite familiy which can be combined to seek new types of magnetic states (Smadici *et al.*, 2007; Bhattacharya *et al.*, 2008; Gibert *et al.*, 2012; Hoffman *et al.*, 2013). For example, many antiferromagnets have ordering temperatures well above room temperature, so one could extend this concept to create interfacial insulating *ferrimagnets* that operate at high temperature (Ueda, Tabata, and Kawai, 1998). Another possibility is to make use of the spatially localized magnetic state in proximity to a metallic layer to create a spin-polarized 2DEG (Nanda and Satpathy, 2008). More broadly, one could create heterostructures with two magnetic materials and use the competition toward different collectively ordered magnetic states in addition to structural incompatibilities to generate a plethora of interesting and potentially spatially varying magnetic phases. These are but a few of the magnetic possibilities which remain to be uncovered at oxide heterointerfaces, chosen to highlight the large phase space still available for exploration and the opportunities available to connect with materials theory in the rational search for new magnetic systems.

V. INTERFACIAL CONTROL OF ORBITAL POLARIZATION

A. The case of rare-earth nickelates

The orbital configuration, i.e., the distribution of the d electrons over the available crystal field levels, plays an important role in the formation of strongly correlated ground states in transition metal oxides (Tokura and Nagaosa, 2000). In general, orbital configurations are closely linked to the structure and may therefore be manipulated at interfaces. Here we discuss these issues specifically for the orthonickelate perovskites $RNiO_3$, where R is a trivalent cation from the

lanthanide series, but the ideas can be extended to other AMO_3 systems.

The original and decade later renewed interest in nickelates arose from the possibility of generating a cupratelike electronic and orbital configuration in a copper-free system (Hamada, 1993; Anisimov, Bukhvalov, and Rice, 1999; Lee and Pickett, 2004; Chaloupka and Khaliullin, 2008; Poltavets *et al.*, 2010). The basic idea is that in bulk $R\mathrm{NiO}_3$ the Ni is octahedrally coordinated, with only small deviations from cubic (O_h) symmetry. Further, formal valence considerations indicate that the nominally Ni^{3+} cation is in the low-spin d^7 configuration, with the t_{2g} states ($d(xy, xz, yz)$) filled and one electron in the twofold degenerate e_g-symmetry ($d(3z^2 - r^2, x^2 - y^2)$) Ni d levels. Low-spin d^7 is a first-order Jahn-Teller configuration, with a susceptibility to bond distortions which break the cubic point symmetry and are enhanced by correlation effects. It was thus expected that modest perturbations would split the e_g levels, leaving an effective one-band configuration where the electron is fully confined to a single orbital.

The degree to which an electron occupies two different m_{l1} and m_{l2} orbitals can be quantified as an orbital polarization

$$P_{l_1 m_{l1}, l_2 m_{l2}} = \frac{n_{l_1 m_{l1}} - n_{l_2 m_{l2}}}{n_{l_1 m_{l1}} + n_{l_2 m_{l2}}},$$

where $n_{l_1 m_{l1}}$ and $n_{l_2 m_{l2}}$ are the occupancies of the $|l_1 m_{l1}\rangle$ and $|l_2 m_{l2}\rangle$ states (Han, Marianetti, and Millis, 2010), with orbital quantum number l_i and magnetic quantum number m_{li}, respectively. For the rare-earth nickelates, the relevant orbital polarization arises from the $n_{x^2-y^2}$ and $n_{3z^2-r^2}$ occupancies, and a fully polarized state $P = 1$ is indicative of a single-band electronic structure.

Something akin to this effect occurs in many members of the "colossal" magnetoresistance manganites, where the basic configuration is a high-spin d^4 configuration and similarly a Jahn-Teller ion that can be manipulated with strain (Tokura and Nagaosa, 2000). Hubbard-model calculations further indicated that the single-band physics was very likely to appear (Hansmann *et al.*, 2009); however, more realistic *ab initio* calculations indicate that the actual electronic configuration for Ni is in the high-spin d^8 state with a hole on the oxygen atom ($d^8\underline{L}$) (Han, Marianetti, and Millis, 2010). Since the high-spin d^8 configuration has one electron in each of the two e_g orbitals, it is significantly less susceptible to undergoing Jahn-Teller distortions, suggesting that it would be more difficult than initially expected to achieve the desired degree of orbital polarization, even in the correlated case (Han *et al.*, 2011). Studies of the dependence of orbital polarization on the different flavors of structural symmetry breaking (Cammarata and Rondinelli, 2013) are thus of great experimental interest and are stringent tests of the theory.

B. Manipulating orbitals in $R\mathrm{NiO}_3$ heterostructures

Advances in high-quality growth of nickelates over the past few years mean that we are now in a position to test these predictions (Tsubouchi *et al.*, 2008; Eguchi *et al.*, 2009; Liu, Kareev, Prosandeev *et al.*, 2010; May *et al.*, 2010; Scherwitzl *et al.*, 2010; Boris *et al.*, 2011; Bruno *et al.*, 2013; Hwang *et al.*, 2013). The basic experimental approach is to use a combination of quantum confinement, achieved by fabricating ultrathin layers of TMO sandwiched between layers of wide-gap insulators, and epitaxial strain, obtained by varying the substrate material, to break the octahedral symmetry. Advanced x-ray techniques are then used to estimate the resulting changes in orbital occupancies.

However, *ab initio* calculations based on density functional theory indicate that the contribution of strain to octahedral symmetry breaking is not completely intuitive [see Rondinelli, May, and Freeland (2012) and references therein]. In particular, a considerable degree of compression or tension can be accommodated by octahedral rotations, without necessarily changing the local point symmetry significantly since the NiO_6 units are highly flexible (Chakhalian *et al.*, 2011). Furthermore, quantum confinement may be affected by the chemistry of the insulating layer, with different degrees of polarization found for different choices of wide-gap insulator (Han, Marianetti, and Millis, 2010).

At present, the experimental results are not completely consistent with each other or with theory. For example, examination of the Ni L_2 edge indicated an ~5% orbital polarization for a single unit cell of LaNiO_3 subject to tensile strain (Freeland *et al.*, 2011) and no orbital polarization for compressive strain. Other measurements employing an orbital reflectometry technique on four unit cell films also observed a similar nonzero interfacial polarization for tensile strain (Benckiser *et al.*, 2011; Frano *et al.*, 2013). Recent studies indicated it is possible to increase the orbital polarization up to 25% through judicious optimization of high tensile strain states and alternative spacer materials (Wu *et al.*, 2013); the latter had been shown theoretically to play a considerable role in obtaining the targeted orbital polarization levels (Han, Marianetti, and Millis, 2010).

C. Open questions in orbital control at interfaces

All experiments agree though that the degree of orbital polarization observed in actual superlattices is small compared to that needed to achieve a fully orbital polarized Ni e_g^1 state. The main challenge is to then build the framework to understand how to create fully orbital polarized states in oxide heterostructures.

One important facet of this problem has to do with strain and symmetry. For example, LaNiO_3 has rhombohedral symmetry in the bulk which actually disfavors a uniaxial Jahn-Teller distortion (Carpenter and Howard, 2009). NdNiO_3, on the other hand, is orthorhombic which allows such a distortion without large energetic penalties. Recent studies by Tung *et al.* (2013) showed that the nickelate films maintain to some extent the symmetry of the bulk, which, due to the connection between compatible lattice distortions and crystal symmetry, directly influences the ability to orbitally polarize the $3d$ states even under large strains.

With this understanding, one may be able to choose the proper bulk symmetry of the TMO to be used in the heterostructure to build in larger orbital polarizations in NdNiO_3 by coupling strain with the interfacial covalency effect discussed above and interfacial proximity effects (Aso *et al.*, 2014; Moon *et al.*, 2014). Even for the case of

$NdNiO_3$ films, however, the orbital polarization is still insufficient to create a fully polarized state (Tung *et al.*, 2013). This is largely due to the energy scale mismatch between elastic strain (~ 100 meV) and the bandwidth (on the order of several electron volts), and the overall tendency to orbital polarization is further reduced by the $d^8\underline{L}$ character of the Ni^{3+} state.

Small orbital polarizations have also been observed even in the case of the Jahn-Teller active manganites (Aruta *et al.*, 2006; Tebano *et al.*, 2008; Pesquera *et al.*, 2012), which indicates that this balancing of drastically different energy scales is difficult even in systems that prefer orbital order. A potential solution is to create interfaces with large symmetry mismatch due to lattice topology or by combination of dissimilar crystal field environments.

Consider, for example, bulk oxides with large orbital polarization such as the cuprates (Chen *et al.*, 1992; Nücker *et al.*, 1995) and Ruddlesden-Popper (layered-structure) nickelates (Pellegrin *et al.*, 1996; Kuiper *et al.*, 1998) as a starting point. In these materials, the large orbital polarization arises from the strongly asymmetric crystal (ligand) field of the layered structure. As discussed for the LCMO and YBCO heterointerface, oxide interfaces can be harnessed to "undo" orbital polarization, but there is no reason why the converse should not also be possible. This offers a real opportunity in the area of matching systems with drastically different symmetries to create orbital states at the interface.

Orbital control can also be used to modulate strongly correlated states. Strain very effectively controls the MIT for $NdNiO_3$ thin films (Liu, Kareev, Gray *et al.*, 2010; Liu *et al.*, 2013), but the underlying mechanism is not fully understood. Using quantum confinement when the layer dimensions approach the atomic limit, it was observed that orbital polarization under compressive strain tends to favor a metallic state while quantum confinement caused a reemergence of a MIT through the interfacial reduction of the orbital polarization (Liu, Kareev *et al.*, 2012). A similar connection was recently observed in the case of VO_2 thin films (Aetukuri *et al.*, 2013), where the decrease in the MIT temperature was correlated with strain driven polarization of the V t_{2g} orbitals. The potential use of strain in combination with symmetry mismatch to tune between correlated metallic and insulating phases is an important issue warranting further investigation.

VI. FERROELECTRIC HETEROSTRUCTURES FROM NONFERROELECTRIC BULK OXIDES

The electrically switchable polarization of ferroelectrics (FE) allows their integration in random access memories (FE-RAM), electro-optical devices, sensing microsystems, active vibration control, and surface acoustic wave systems, to high frequency devices (Setter *et al.*, 2006). The main challenges for future FE-RAM scaling, however, are that the FE dielectric thickness must be reduced to fit within the required device area while maintaining sufficient reproducibility and signal margins for sense amplifier differentiation between a "0" and "1" data state (Wu *et al.*, 2010). Furthermore, nondestructive *magnetic* sensing of *electric* polarization, enhanced miniaturization, and increased packaging density in magnetoelectric (ME) materials (Fiebig, 2005; Eerenstein, Mathur, and Scott, 2006; Ramesh and Spaldin, 2007; Velev, Jaswal, and Tsymbal, 2011) enabled the realization of four-state logic in a single device (Bibes and Barthelemy, 2008; Khomskii, 2009).

The conventional approach for realizing strong ME materials, i.e., where their is strong coupling between the primary electric and magnetic polarizations, uses naturally occurring materials possessing primary ferroic orders, namely, ferroelectricity and ferromagnetism. Such materials not only are rare, but often suffer from weak coupling between the spin and charge degrees of freedom (Eerenstein, Mathur, and Scott, 2006).

Recent advances in atomic layer epitaxy now enable the design and fabrication of heterostructures with atomically flat interfaces that can support new forms of ferroelectricity (Bousquet *et al.*, 2008; Rondinelli and Fennie, 2012; Mulder *et al.*, 2013) and magnetoelectric coupling owing to interfacial interactions among electronic spins, charges, and orbitals (Wu *et al.*, 2010). A promising avenue to pursue in the search for new materials with emergent ferroelectricity and a strong magnetic field dependence of the electric polarization exploits a superlattice structure with broken inversion symmetry, which results from being constructed from three distinct layers (Warusawithana *et al.*, 2003; Lee *et al.*, 2005). The "tricolor" layering lifts inversion symmetry (a prerequisite for an electric polarization) whereas epitaxial strain applied to the heterostructure can promote the formation of electrically and magnetically tunable polarizations, even in the absence of ferroic components (Hatt and Spaldin, 2007; Tokura, 2007).

Using a combination of complementary experimental probes, magnetoelectricity was recently demonstrated in artificial trilayer heterostructures consisting solely of dielectric antiferromagnetic oxides [Fig. 5(a)]. Laser molecular-beam epitaxy was used to create the heterostructure comprising alternating $LaMnO_3$, $SrMnO_3$, and $NdMnO_3$ layers on a $SrTiO_3$ substrate. Rogdakis *et al.* (2012) reported the emergence of ferroelectricity below 40 K [Fig. 5(c)] and it was found to depend on the number of $NdMnO_3$ layers n in the superlattice [Fig. 5(d)]. Interestingly, they observed slim looplike polarization–electric (P-E) field hysteresis, with an extended tail of the polarization above the ferroelectric transition temperature and a thermal hysteresis between zero-field-cooled and field-cooled measurements. Such features are typical of relaxor ferroelectrics and were attributed to interface effects (Rogdakis *et al.*, 2012). We note that this dielectric relaxation also leads to differences in the magnitudes of the measured polarization obtained from the P-E loop and the pyrocurrent measurement, which might also be affected from the challenges in characterizing the dielectric properties of ultrathin film oxides with techniques commonly used for bulk single crystals. Nonetheless, the magnetoelectric coupling resulted in 150% magnetic modulation of the electric polarization, demonstrating how heterostructuring multiple compounds together to lift inversion symmetry in superlattices is an avenue to create new functionalities.

First-principles density functional calculations indicated that broken space inversion symmetry and mixed valency, arising from the heterostructure geometry (cation layer

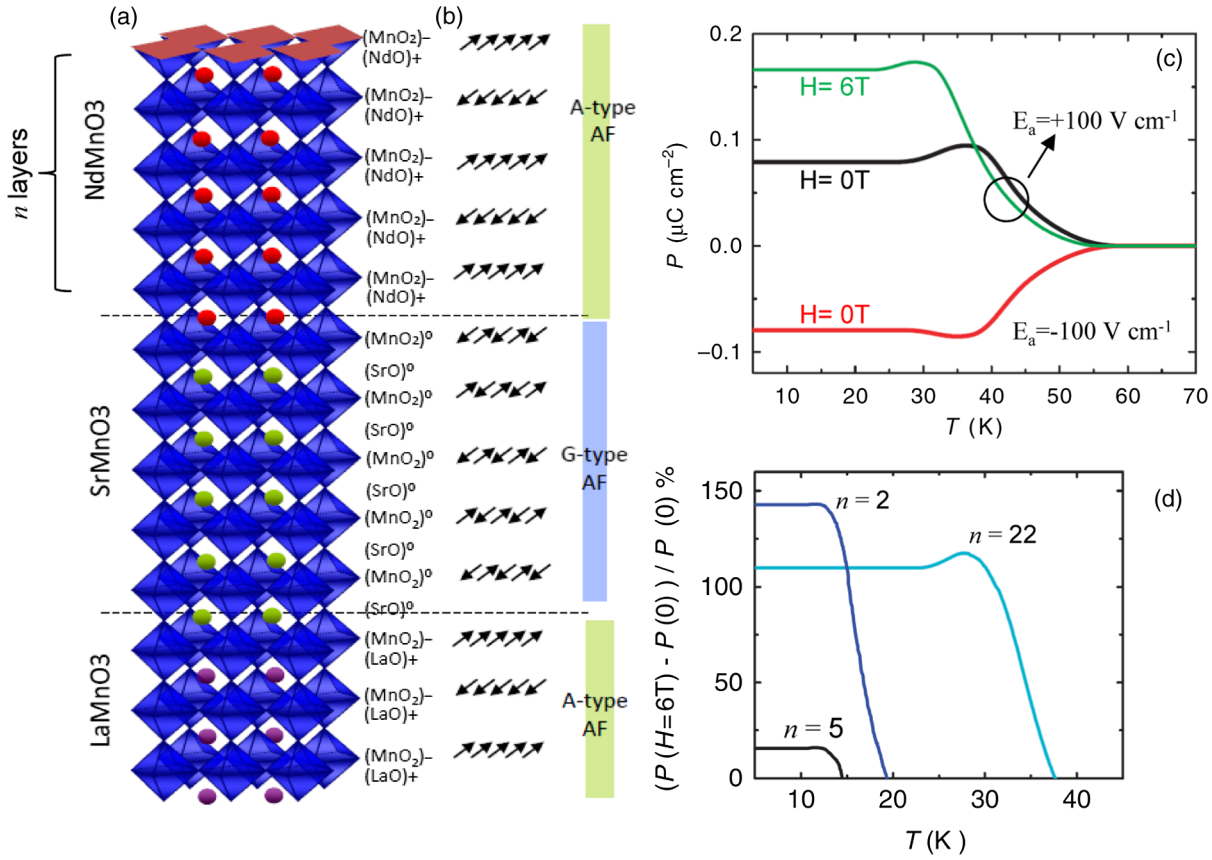

FIG. 5 (color online). Ferroelectric and magnetoelectric properties of the $[(NdMnO_3)_n/(SrMnO_3)_n/(LaMnO_3)_n]_m$ superlattice, where (n, m) denotes the specfic superlattice structure. (a) Schematic $[(NdMnO_3)_5/(SrMnO_3)_5/(LaMnO_3)_5]_8$ superlattice on single-crystalline $SrTiO_3$ substrate with the metal-oxygen octahedra and A cations emphasized. The arrays of the arrows in (b) represent the corresponding antiferromagnetic spin arrangements for each component of the heterostructure. (c) Temperature (T) dependence of the electric polarization (P) measured in a superlattice of period (22,2) using the pyroelectric technique for a typical electric field (E_a) of $+100\ \mathrm{V\,cm^{-1}}$ (middle curve) and $-100\ \mathrm{V\,cm^{-1}}$ (bottom curve) applied perpendicular to the plane of the superlattice layering. The temperature-dependent electric polarization under a magnetic field $H = 6$ T applied parallel to the plane of the superlattice layering (top curve) reveals strong magnetoelectric coupling. (d) Normalized relative change in the electric polarization at fixed electric and magnetic fields for various superlattices. Adapted Rogdakis *et al.*, 2012.

sequence) and interfacial polar discontinuity, respectively, are responsible for the observed behavior. In particular, the formal charge layering of the $LaMnO_3$ and $NdMnO_3$ components at the interfaces with $SrMnO_3$ gives rise to a charge discontinuity, leading to electron transfer and cooperative off centering of the cations. The A-cation layering leads to a pattern of Mn and A-cation displacements along the superlattice normal growth direction that lift inversion symmetry and therefore produce the macroscopic electric polarization. We note that the ferroelectric relaxor behavior could not be seen from the theoretical results, which capture the static and cation ordered zero-temperature behavior.

This work demonstrates yet another fascinating example of emergent functionality exhibited in heterostructures. The ability to lift inversion symmetry and independently tune spin order allows the design of many more materials with multifunctional behavior (Gou and Rondinelli, 2014; Puggioni and Rondinelli, 2014). One may exploit these systems to engineer devices from artificial low-dimensional materials exhibiting novel tunable functions distinct from that of bulk systems.

VII. CONCLUSION

The physics of interfaces between materials exhibiting correlated electronic behaviors including superconductivity, magnetism, and ferroelectricity is a rapidly advancing field, situated at the intersection of materials science, solid-state chemistry, and condensed matter physics. Understanding and exploiting these remarkable systems places extraordinary demands on synthesis, measurement, and theory, and the challenge is stimulating remarkable work in all areas. By way of conclusion we highlight challenges and prospects in correlated oxide interfaces.

A. Chemical and structural order

Characterization and control of chemical and structural order is a crucial issue. While research to date has revealed remarkable phenomena, clearly related to properties of theoretically ideal interfaces, effects of disorder are not negligible. The brutally short length scales (often only one or two unit cells) pose strong constraints on materials quality. For example, metal-to-insulator transitions generically occur in

oxide heterstructures when the thickness of the metallic layer becomes of the order of 1–2 unit cells. Systematic dependence on strain (Son *et al.*, 2010) and systematic evolution of electronic structure with thickness (Yoshimatsu *et al.*, 2011) suggest an important intrinsic component, but disorder effects and changes in growth processes on these length scales cannot yet be ruled out as mechanisms. Antisite defects mean that real interfaces are not as sharp as depicted in the idealized sketches shown in this Colloquium, and these defects are not necessarily easy to identify in transmission electron microscopy experiments, which average over columns of order 10^3 atoms. Further, oxygen defects and interstitials play a crucial role in transition metal oxides and oxygen partial pressure during growth and in postgrowth annealing of heterostructures clearly affects properties in many cases (Nakagawa, Hwang, and Muller, 2006; Ariando *et al.*, 2011). Methods to further define and control the actual structure of interfaces are urgently needed. One area of future study is to couple the insight from *in situ* studies of oxide film synthesis to that of multiscale theory in order to build a mechanistic understanding of the process by which interfaces are created.

B. Theory

The importance and interest of oxide interfaces for the general issue of the theory of correlated electron materials cannot be overemphasized. Understanding the phenomena at interfaces requires a combination of sophisticated many-body physics (to understand the correlated electron states) and *ab initio* insights (to understand the implications of the changes in octahedral rotations, atomic coordination, and lattice relaxations). The present state of the theoretical art is a combination of the analysis of model systems (in particular, the Hubbard model), which cannot easily encode many real materials aspects, in particular, the transition metal and ligand covalence as well as the energetics associated with lattice relaxations and *ab initio* techniques (especially the DFT + U method) which have provided crucial insight but are based on a greatly oversimplified Hartree approximation to the many-body physics and may overemphasize order (Chan, Werner, and Millis, 2009; Wang *et al.*, 2012). In particular, the status of the DFT + U predictions of magnetism (Okamoto, Millis, and Spaldin, 2006) and charge order (Pentcheva and Pickett, 2007) at the LAO and STO interface remains unclear.

The combination of density functional band theory and dynamical mean field theory (DFT + DMFT) is a promising alternative (Kotliar *et al.*, 2006), combining *ab initio* and many-body physics in a systematic way. However, working implementations of total energy calculations are only now beginning to appear (Park, Millis, and Marianetti, 2013) and forces cannot yet be computed so structural optimization remains a challenge. More fundamentally, existing implementations for systems in which more than one d orbital is important are based on the single-site approximation, which is believed to become poor in the two-dimensional situation relevant to heterostructures.

C. Topological states of matter

Topological insulators (TIs) are a fascinating class of materials in which strong spin-orbit interaction promotes gapless electronic states on the surface (i.e., edge states) with the bulk of a material remaining gapped (Fu, Kane, and Mele, 2007; Hsieh *et al.*, 2008; Hasan and Kane, 2010; Moore, 2010; Qi and Zhang, 2010). Most of the current TI materials belong to the Bi_2X_3 (X = Se, Te) family. Recently, a new approach was proposed that is based on superlattices of two (or three) unit cells of a strongly correlated electron perovskite ABO_3 grown along the [111] direction combined with a band insulator spacer layer; the resulting heterostructure structurally forms a buckled honeycomb lattice topologically equivalent to that of graphene lattice for the case of two unit cell strongly correlated oxide. Depending on the strength of electron-electron correlations, the magnitude of Hund's coupling, and intersite hopping, the proposed heterostructures display potentially rich physics associated with exotic electronic and topological phases (Rüegg and Fiete, 2011; Xiao *et al.*, 2011; Yang *et al.*, 2011; Rüegg *et al.*, 2012, 2013; Okamoto, 2013; Okamoto *et al.*, 2014). At present, the main challenge in experimental realization is the film growth along the [111] direction since for the commonly used substrates, e.g., $SrTiO_3$, $LaAlO_3$, $NdGaO_3$, $YAlO_3$, etc., the (111) structure consists of alternating $\pm 4e$ or $\pm 3e$ charged planes along this direction. The large polar discontinuity generally results in complex surface and interface and electronic reconstructions (Marks *et al.*, 2009; Enterkin *et al.*, 2010), which can act to compensate for the polar mismatch. To date there is limited understanding of thin film nucleation, growth, and charge compensation in perovskites along highly polar directions. Very recently the synthesis work in this direction was initiated (Gibert *et al.*, 2012; Liu *et al.*, 2014; Middey *et al.*, 2012, 2014).

D. Oxygen defect control

While many of the examples discussed involve oxygen stoichiometric perovskites, the ease of removal and/or the addition of oxygen can also offer opportunities for materials that can be programed by their chemical environment (Kalinin, Borisevich, and Fong, 2012; Kalinin and Spaldin, 2013). While the role of oxygen vacancies has been explored deeply in the context of catalysis and fuel cells (Adler, 2004), recent work has highlighted the controlled stabilization of related oxygen deficient phases using oxide heterostructures. This is interesting for epitaxial thin film phases such as $SrCoO_{3-\delta}$ (Jeen *et al.*, 2013; Jeen, Choi *et al.*, 2013) or $La_{1-x}Sr_xFeO_{3-\delta}$ (Xie *et al.*, 2013), which can be reversibly converted between oxygen deficient and stoichiometric phases at low temperatures. Since these phases have drastically different ground states, it offers an interesting path for control of strongly correlated electrons via dynamic anion compositional control. By combining low conversion energy with electrochemical gating of vacancies, such as that seen recently for VO_2 (Jeong *et al.*, 2013) and $RNiO_3$ (Shi *et al.*, 2013), this approach allows direct control of the metal versus insulating phase as well as possible elements of brainlike (neuromorphic) electronic circuits.

E. Moving beyond the static realm

Up to now, all the properties that have been discussed were limited to the quasiequilibrium properties, but in the future one should also investigate the *dynamical* degree of freedom to explore the emergence of unique transient states. While the dynamic response for bulk materials has been extensively investigated (Averitt and Taylor, 2002; Basov, 2005; Zhang and Averitt, 2014), oxide heterostructures offer new possibilities. Recent pump-probe studies of oxide films illustrate the potential for ultrafast strain modulation (Daranciang *et al.*, 2012; Wen *et al.*, 2013), which allows one to manipulate the lattice in a new direction since the film motion is clamped in plane by epitaxy and can alter the lattice only out of plane. Using this epitaxial constraint allows one to drive the crystalline lattice (symmetry, rotations, etc.) into distinctly different areas of phase space. For example, experiments in manganite thin films showed the emergence of a hidden phase that existed only in the dynamic realm (Ichikawa *et al.*, 2011). Moving into the mid-IR region enables direct pumping of lattice modes that can trigger phase transitions (Rini *et al.*, 2007) and was recently used to trigger a metal-insulator transition through dynamic strain created by direct pumping of substrate phonons (Caviglia *et al.*, 2012). Low energy photons in the terahertz regime can also serve as a dynamic way to drive transitions with ultrafast electric fields (M. Liu *et al.*, 2012). Such experiments have only begun to explore the complex landscape available in the dynamic realm.

ACKNOWLEDGMENTS

The work at Argonne National Laboratory, including the Advanced Photon Source, is supported by the U.S. Department of Energy, Office of Science under Grant No. DEAC02-06CH11357. J. C. was supported by DOD-ARO under Grant No. 0402-17291. The work in Singapore was supported by the National Research Foundation, Singapore, through Grant No. NRF-CRP4-2008-04. J. M. R. was supported by ARO (No. W911NF-12-1-0133) and acknowledges useful discussions leading to ideas presented in this manuscript during a workshop sponsored by the Army Research Office (Grant No. W911NF-12-1-0171). A. J. M. acknowledges the U.S. Department of Energy, Office of Science, under Grant No. DE-FG02-04ER46169.

REFERENCES

Adler, S. B., 2004, Chem. Rev. **104**, 4791.
Aetukuri, N. B., *et al.*, 2013, Nat. Phys. **9**, 661.
Ahn, C. H., J. M. Triscone, and J. Mannhart, 2003, Nature (London) **424**, 1015.
Ahn, C. H., *et al.*, 2006, Rev. Mod. Phys. **78**, 1185.
Anderson, P., 1950, Phys. Rev. **79**, 350.
Anisimov, V., D. Bukhvalov, and T. Rice, 1999, Phys. Rev. B **59**, 7901.
Ariando, *et al.*, 2011, Nat. Commun. **2**, 188.
Armitage, N., P. Fournier, and R. Greene, 2010, Rev. Mod. Phys. **82**, 2421.
Aruta, C., G. Ghiringhelli, A. Tebano, N. Boggio, N. Brookes, P. Medaglia, and G. Balestrino, 2006, Phys. Rev. B **73**, 235121.
Aso, R., D. Kan, Y. Shimakawa, and H. Kurata, 2014, Cryst. Growth Des. **14**, 2128.
Averitt, R. D., and A. J. Taylor, 2002, J. Phys. Condens. Matter **14**, R1357.
Basov, D. N., 2005, Rev. Mod. Phys. **77**, 721.
Benckiser, E., *et al.*, 2011, Nat. Mater. **10**, 189.
Bert, J. A., B. Kalisky, C. Bell, M. Kim, Y. Hikita, H. Y. Hwang, and K. A. Moler, 2011, Nat. Phys. **7**, 767.
Bhattacharya, A., S. J. May, S. G. E. te Velthuis, M. Warusawithana, X. Zhai, B. Jiang, J. M. Zuo, M. R. Fitzsimmons, S. D. Bader, and J. N. Eckstein, 2008, Phys. Rev. Lett. **100**, 257203.
Bibes, M., and A. Barthelemy, 2008, Nat. Mater. **7**, 425.
Bibes, M., J. E. Villegas, and A. Barthelemy, 2011, Adv. Phys. **60**, 5.
Biscaras, J., N. Bergeal, S. Hurand, C. Grossetête, A. Rastogi, R. C. Budhani, D. Leboeuf, C. Proust, and J. Lesueur, 2012, Phys. Rev. Lett. **108**, 247004.
Boris, A. V., *et al.*, 2011, Science **332**, 937.
Bousquet, E., M. Dawber, N. Stucki, C. Lichtensteiger, P. Hermet, S. Gariglio, J.-M. Triscone, and P. Ghosez, 2008, Nature (London) **452**, 732.
Brinkman, A., M. Huijben, M. van Zalk, J. Huijben, U. Zeitler, J. C. Maan, W. G. van der Wiel, G. Rijnders, D. H. A. Blank, and H. Hilgenkamp, 2007, Nat. Mater. **6**, 493.
Bruno, F. Y., *et al.*, 2013, Phys. Rev. B **88**, 195108.
Cammarata, A., and J. M. Rondinelli, 2013, Phys. Rev. B **87**, 155135.
Carpenter, M. A., and C. J. Howard, 2009, Acta Crystallogr. Sect. B **65**, 134.
Caviglia, A., *et al.*, 2012, Phys. Rev. Lett. **108**, 136801.
Caviglia, A. D., S. Gariglio, N. Reyren, D. Jaccard, T. Schneider, M. Gabay, S. Thiel, G. Hammerl, J. Mannhart, and J. M. Triscone, 2008, Nature (London) **456**, 624.
Chakhalian, J., J. W. Freeland, H.-U. Habermeier, G. Cristiani, G. Khaliullin, M. van Veenendaal, and B. Keimer, 2007, Science **318**, 1114.
Chakhalian, J., *et al.*, 2006, Nat. Phys. **2**, 244.
Chakhalian, J., *et al.*, 2011, Phys. Rev. Lett. **107**, 116805.
Chaloupka, J., and G. Khaliullin, 2008, Phys. Rev. Lett. **100**, 016404.
Chan, C.-K., P. Werner, and A. J. Millis, 2009, Phys. Rev. B **80**, 235114.
Charlebois, M., S. R. Hassan, R. Karan, D. Sénéchal, and A.-M. S. Tremblay, 2013, Phys. Rev. B **87**, 035137.
Chen, C., L. Tjeng, J. Kwo, H. Kao, P. Rudolf, F. Sette, and R. Fleming, 1992, Phys. Rev. Lett. **68**, 2543.
Chen, R., S. Lee, and L. Balents, 2013, Phys. Rev. B **87**, 161119.
Chien, T. Y., L. F. Kourkoutis, J. Chakhalian, B. Gray, M. Kareev, N. P. Guisinger, D. A. Muller, and J. W. Freeland, 2013, Nat. Commun. **4**, 2336.
Chiorescu, C., J. Cohn, and J. Neumeier, 2007, Phys. Rev. B **76**, 020404.
Dagotto, E., T. Hotta, and A. Moreo, 2001, Phys. Rep. **344**, 1.
Daranciang, D., *et al.*, 2012, Phys. Rev. Lett. **108**, 087601.
Dekker, M., A. Herklotz, L. Schultz, M. Reibold, K. Vogel, M. Biegalski, H. Christen, and K. Dörr, 2011, Phys. Rev. B **84**, 054463.
Driza, N., *et al.*, 2012, Nat. Mater. **11**, 675.
Eerenstein, W., N. D. Mathur, and J. F. Scott, 2006, Nature (London) **442**, 759.
Eguchi, R., A. Chainani, M. Taguchi, M. Matsunami, Y. Ishida, K. Horiba, Y. Senba, H. Ohashi, and S. Shin, 2009, Phys. Rev. B **79**, 115122.
Eng, H. W., P. W. Barnes, B. M. Auer, and P. M. Woodward, 2003, J. Solid State Chem. **175**, 94.
Enterkin, J. A., A. K. Subramanian, B. C. Russell, M. R. Castell, K. R. Poeppelmeier, and L. D. Marks, 2010, Nat. Mater. **9**, 245.

Fiebig, M., 2005, J. Phys. D **38**, R123.
Frano, A., *et al.*, 2013, Phys. Rev. Lett. **111**, 106804.
Freeland, J., K. Gray, L. Ozyuzer, P. Berghuis, E. Badica, J. Kavich, H. Zheng, and J. Mitchell, 2005, Nat. Mater. **4**, 62.
Freeland, J. W., J. Liu, M. Kareev, B. Gray, J. W. Kim, P. Ryan, R. Pentcheva, and J. Chakhalian, 2011, Europhys. Lett. **96**, 57004.
Freeland, J. W., J. X. Ma, and J. Shi, 2008, Appl. Phys. Lett. **93**, 212501.
Freeland, J. W., *et al.*, 2010, Phys. Rev. B **81**, 094414.
Fu, L., C. Kane, and E. Mele, 2007, Phys. Rev. Lett. **98**, 106803.
Fuchs, D., C. Pinta, T. Schwarz, P. Schweiss, P. Nagel, S. Schuppler, R. Schneider, M. Merz, G. Roth, and H. von Loehneysen, 2007, Phys. Rev. B **75**, 144402.
Garcia-Barriocanal, J., A. M. Perez-Muñoz, Z. Sefrioui, D. Arias, M. Varela, C. Leon, S. J. Pennycook, and J. Santamaria, 2013, Phys. Rev. B **87**, 245105.
Gertner, J., 2013, *The Idea Factory: Bell Labs and the Great Age of American Innovation* (Penguin, New York).
Gibert, M., P. Zubko, R. Scherwitzl, J. I. Íñiguez, and J.-M. Triscone, 2012, Nat. Mater. **11**, 195.
Goodenough, J. B., 1955, Phys. Rev. **100**, 564.
Gou, G., and J. M. Rondinelli, 2014, Adv. Mater. Interfaces **1**, 1400042.
Granozio, F. M., G. Koster, and G. Rijnders, 2013, MRS Bull. **38**, 1017.
Grutter, A. J., *et al.*, 2013, Phys. Rev. Lett. **111**, 087202.
Hamada, N., 1993, J. Phys. Chem. Solids **54**, 1157.
Han, M. J., C. A. Marianetti, and A. J. Millis, 2010, Phys. Rev. B **82**, 134408.
Han, M. J., X. Wang, C. A. Marianetti, and A. J. Millis, 2011, Phys. Rev. Lett. **107**, 206804.
Hansmann, P., X. Yang, A. Toschi, G. Khaliullin, O. K. Andersen, and K. Held, 2009, Phys. Rev. Lett. **103**, 016401.
Harris, J., J. Clegg, R. Beall, J. Castagné, K. Woodbridge, and C. Roberts, 1991, J. Cryst. Growth **111**, 239.
Hasan, M. Z., and C. L. Kane, 2010, Rev. Mod. Phys. **82**, 3045.
Hatt, A. J., and N. A. Spaldin, 2007, Appl. Phys. Lett. **90**, 242916.
He, C., *et al.*, 2012, Phys. Rev. Lett. **109**, 197202.
Herranz, G., *et al.*, 2007, Phys. Rev. Lett. **98**, 216803.
Hikita, Y., M. Nishikawa, T. Yajima, and H. Y. Hwang, 2009, Phys. Rev. B **79**, 073101.
Hoffman, J., I. C. Tung, B. B. Nelson-Cheeseman, M. Liu, J. W. Freeland, and A. Bhattacharya, 2013, Phys. Rev. B **88**, 144411.
Hoffmann, A., S. T. Velthuis, Z. Sefrioui, J. Santamaría, M. Fitzsimmons, S. Park, and M. Varela, 2005, Phys. Rev. B **72**, 140407.
Holden, T., *et al.*, 2004, Phys. Rev. B **69**, 064505.
Hoppler, J., *et al.*, 2009, Nat. Mater. **8**, 315.
Hotta, Y., T. Susaki, and H. Hwang, 2007, Phys. Rev. Lett. **99**, 236805.
Hsieh, D., D. Qian, L. Wray, Y. Xia, Y. S. Hor, R. J. Cava, and M. Z. Hasan, 2008, Nature (London) **452**, 970.
Hwang, H. Y., Y. Iwasa, M. Kawasaki, B. Keimer, N. Nagaosa, and Y. Tokura, 2012, Nat. Mater. **11**, 103.
Hwang, J., J. Son, J. Y. Zhang, A. Janotti, C. G. Van de Walle, and S. Stemmer, 2013, Phys. Rev. B **87**, 060101.
Ichikawa, H., *et al.*, 2011, Nat. Mater. **10**, 101.
Imada, M., A. Fujimori, and Y. Tokura, 1998, Rev. Mod. Phys. **70**, 1039.
Jeen, H., W. S. Choi, J. W. Freeland, H. Ohta, C. U. Jung, and H. N. Lee, 2013, Adv. Mater. **25**, 3651.
Jeen, H., *et al.*, 2013, Nat. Mater. **12**, 1057.
Jeong, J., N. Aetukuri, T. Graf, T. D. Schladt, M. G. Samant, and S. S. P. Parkin, 2013, Science **339**, 1402.
Jin, K., P. Bach, X. H. Zhang, U. Grupel, E. Zohar, I. Diamant, Y. Dagan, S. Smadici, P. Abbamonte, and R. L. Greene, 2011, Phys. Rev. B **83**, 060511.
Kalcheim, Y., T. Kirzhner, G. Koren, and O. Millo, 2011, Phys. Rev. B **83**, 064510.
Kalinin, S. V., A. Borisevich, and D. Fong, 2012, ACS Nano **6**, 10 423.
Kalinin, S. V., and N. A. Spaldin, 2013, Science **341**, 858.
Kanamori, J., 1959, J. Phys. Chem. Solids **10**, 87.
Kareev, M., Y.Cao, X. Liu, S. Middey, D. Meyers, and J. Chakhalian, 2013, Appl. Phys. Lett. **103**, 231605.
Kavich, J. J., M. P. Warusawithana, J. W. Freeland, P. Ryan, X. Zhai, R. H. Kodama, and J. N. Eckstein, 2007, Phys. Rev. B **76**, 014410.
Khomskii, D., 2009, Physics **2**, 20.
Khomskii, D., and G. Sawatzky, 1997, Solid State Commun. **102**, 87.
Kotliar, G., S. Savrasov, K. Haule, V. Oudovenko, O. Parcollet, and C. Marianetti, 2006, Rev. Mod. Phys. **78**, 865.
Kuiper, P., J. V. Elp, D. Rice, D. Buttrey, H.-J. Lin, and C. Chen, 1998, Phys. Rev. B **57**, 1552.
Lee, H. N., H. M. Christen, M. F. Chisholm, C. M. Rouleau, and D. H. Lowndes, 2005, Nature (London) **433**, 395.
Lee, J. H., *et al.*, 2010, Nature (London) **466**, 954.
Lee, K.-W., and W. Pickett, 2004, Phys. Rev. B **70**, 165109.
Lee, P. A, and X.-G. Wen, 2006, Rev. Mod. Phys. **78**, 17.
Lee, W.-C., and A. Macdonald, 2006, Phys. Rev. B **74**, 075106.
Lee, W.-C., and A. Macdonald, 2007, Phys. Rev. B **76**, 075339.
Li, L., C. Richter, J. Mannhart, and R. C. Ashoori, 2011, Nat. Phys. **7**, 762.
Liu, J., M. Kareev, B. Gray, J. W. Kim, P. Ryan, B. Dabrowski, J. W. Freeland, and J. Chakhalian, 2010, Appl. Phys. Lett. **96**, 233110.
Liu, J., M. Kareev, D. Meyers, B. Gray, P. Ryan, J. Freeland, and J. Chakhalian, 2012, Phys. Rev. Lett. **109**, 107402.
Liu, J., M. Kareev, S. Prosandeev, B. Gray, P. Ryan, J. W. Freeland, and J. Chakhalian, 2010, Appl. Phys. Lett. **96**, 133111.
Liu, J., *et al.*, 2013, Nat. Commun. **4**, 2714.
Liu, M., *et al.*, 2012, Nature (London) **487**, 345.
Liu, X., M. Kareev, Y. Cao, J. Liu, S. Middey, D. Meyers, J. W. Freeland, and J. Chakhalian, 2014, Appl. Phys. Lett. **105**, 042401.
Mackenzie, A. P., 2003, Rev. Mod. Phys. **75**, 657.
Mannhart, J., D. A. Blank, H. Y. Hwang, A. J. Millis, and J. M. Triscone, 2008, MRS Bull. **33**, 1027.
Mannhart, J., and D. Schlom, 2010, Science **327**, 1607.
Marks, L. D., A. N. Chiaramonti, F. Tran, and P. Blaha, 2009, Surf. Sci. **603**, 2179.
May, S. J., J. W. Kim, J. M. Rondinelli, E. Karapetrova, N. A. Spaldin, A. Bhattacharya, and P. J. Ryan, 2010, Phys. Rev. B **82**, 014110.
May, S. J., A. B. Shah, S. G. E. te Velthuis, M. R. Fitzsimmons, J. M. Zuo, X. Zhai, J. N. Eckstein, S. D. Bader, and A. Bhattacharya, 2008, Phys. Rev. B **77**, 174409.
May, S. J., *et al.*, 2009, Nat. Mater. **8**, 892.
Middey, S., D. Meyers, D. Doennig, M. Kareev, X. Liu, Y. Cao, P. Ryan, R. Pentcheva, J. W. Freeland, and J. Chakhalian, 2014, arXiv:1407.1570.
Middey, S., D. Meyers, M. Kareev, E. J. Moon, B. A. Gray, X. Liu, J. W. Freeland, and J. Chakhalian, 2012, Appl. Phys. Lett. **101**, 261602.
Moetakef, P., C. A. Jackson, J. Hwang, L. Balents, S. J. Allen, and S. Stemmer, 2012, Phys. Rev. B **86**, 201102.

Moon, E. J., P. V. Balachandran, B. J. Kirby, D. J. Keavney, R. J. Sichel-Tissot, C. M. Schlepütz, E. Karapetrova, X. M. Cheng, J. M. Rondinelli, and S. J. May, 2014, Nano Lett. **14**, 2509.
Moore, J. E., 2010, Nature (London) **464**, 194.
Mulder, A. T., N. A. Benedek, J. M. Rondinelli, and C. J. Fennie, 2013, Adv. Funct. Mater. **23**, 4810.
Nakagawa, N., H. Hwang, and D. Muller, 2006, Nat. Mater. **5**, 204.
Nanda, B. R. K., and S. Satpathy, 2008, Phys. Rev. Lett. **101**, 127201.
Nanda, B. R. K., S. Satpathy, and M. S. Springborg, 2007, Phys. Rev. Lett. **98**, 216804.
Neumeier, J., and J. Cohn, 2000, Phys. Rev. B **61**, 14 319.
Nücker, N., E. Pellegrin, P. Schweiss, J. Fink, S. Molodtsov, C. Simmons, G. Kaindl, W. Frentrup, A. Erb, and G. Müller-Vogt, 1995, Phys. Rev. B **51**, 8529.
Ohtomo, A., and H. Y. Hwang, 2004, Nature (London) **427**, 423.
Ohtomo, A., D. A. Muller, J. L. Grazul, and H. Y. Hwang, 2002, Nature (London) **419**, 378.
Oka, T., and N. Nagaosa, 2005, Phys. Rev. Lett. **95**, 266403.
Okamoto, S., 2013, Phys. Rev. Lett. **110**, 066403.
Okamoto, S., A. Millis, and N. Spaldin, 2006, Phys. Rev. Lett. **97**, 056802.
Okamoto, S., and A. J. Millis, 2004, Nature (London) **428**, 630.
Okamoto, S., W. ZhuY. NomuraR. AritaD. Xiao, and N. Nagaosa, 2014, Phys. Rev. B **89**, 195121.
Ovchinnikov, S. G., 2003, Phys. Usp. **46**, 21.
Park, H., A. J. Millis, and C. A. Marianetti, 2013, arXiv:1310.5772.
Park, J., *et al.*, 2013, Phys. Rev. Lett. **110**, 017401.
Park, S., P. Ryan, E. Karapetrova, J. W. Kim, J. X. Ma, J. Shi, J. W. Freeland, and W. Wu, 2009, Appl. Phys. Lett. **95**, 072508.
Pellegrin, E., J. Zaanen, H.-J. Lin, G. Meigs, C. Chen, G. Ho, H. Eisaki, and S. Uchida, 1996, Phys. Rev. B **53**, 10 667.
Peña, V., Z. Sefrioui, D. Arias, C. Leon, J. Santamaria, J. Martinez, S. T. Velthuis, and A. Hoffmann, 2005, Phys. Rev. Lett. **94**, 057002.
Peña, V., Z. Sefrioui, D. Arias, C. Leon, J. Santamaria, M. Varela, S. Pennycook, and J. Martinez, 2004, Phys. Rev. B **69**, 224502.
Pentcheva, R., and W. E. Pickett, 2007, Phys. Rev. Lett. **99**, 016802.
Pesquera, D., G. Herranz, A. Barla, E. Pellegrin, F. Bondino, E. Magnano, F. Sánchez, and J. Fontcuberta, 2012, Nat. Commun. **3**, 1189.
Poltavets, V. V., *et al.*, 2010, Phys. Rev. Lett. **104**, 206403.
Puggioni, D., and J. M. Rondinelli, 2014, Nat. Commun. **5**, 3432.
Qi, X.-L., and S.-C. Zhang, 2010, Phys. Today **63**, No. 1, 33.
Ramesh, R., and N. A. Spaldin, 2007, Nat. Mater. **6**, 21.
Reyren, N., *et al.*, 2007, Science **317**, 1196.
Rini, M., R. Tobey, N. Dean, J. Itatani, Y. Tomioka, Y. Tokura, R. W. Schoenlein, and A. Cavalleri, 2007, Nature (London) **449**, 72.
Rogdakis, K., J. W. Seo, Z. Viskadourakis, Y. Wang, L. F. N. A. Qune, E. Choi, J. D. Burton, E. Y. Tsymbal, J. Lee, and C. Panagopoulos, 2012, Nat. Commun. **3**, 1064.
Rondinelli, J., S. May, and J. Freeland, 2012, MRS Bull. **37**, 261.
Rondinelli, J. M., and C. J. Fennie, 2012, Adv. Mater. **24**, 1961.
Rondinelli, J. M., and N. A. Spaldin, 2009, Phys. Rev. B **79**, 054409.
Rüegg, A., and G. Fiete, 2011, Phys. Rev. B **84**, 201103.
Rüegg, A., C. Mitra, A. Demkov, and G. Fiete, 2012, Phys. Rev. B **85**, 245131.
Rüegg, A., C. Mitra, A. A. Demkov, and G. A. Fiete, 2013, Phys. Rev. B **88**, 115146.
Salluzzo, M., S. Gariglio, X. Torrelles, Z. Ristic, R. D. Capua, J. Drnec, M. M. Sala, G. Ghiringhelli, R. Felici, and N. B. Brookes, 2013, Adv. Mater. **25**, 2333.
Satapathy, D., *et al.*, 2012, Phys. Rev. Lett. **108**, 197201.
Savoia, A., *et al.*, 2009, Phys. Rev. B **80**, 075110.
Scherwitzl, R., P. Zubko, I. G. Lezama, S. Ono, A. F. Morpurgo, G. Catalan, and J.-M. Triscone, 2010, Adv. Mater. **22**, 5517.
Schlom, D. G., L.-Q. Chen, X. Pan, A. Schmehl, and M. A. Zurbuchen, 2008, J. Am. Ceram. Soc. **91**, 2429.
Schubert, E. F., 1990, J. Vac. Sci. Technol. A **8**, 2980.
Sefrioui, Z., D. Arias, V. Peña, J. Villegas, M. Varela, P. Prieto, C. León, J. Martinez, and J. Santamaria, 2003, Phys. Rev. B **67**, 214511.
Seo, J. W., *et al.*, 2010, Phys. Rev. Lett. **105**, 167206.
Setter, N., *et al.*, 2006, J. Appl. Phys. **100**, 051606.
Shi, J., S. D. Ha, Y. Zhou, F. Schoofs, and S. Ramanathan, 2013, Nat. Commun. **4**, 2676.
Sing, M., *et al.*, 2009, Phys. Rev. Lett. **102**, 176805.
Smadici, S., P. Abbamonte, A. Bhattacharya, X. Zhai, B. Jiang, A. Rusydi, J. N. Eckstein, S. D. Bader, and J.-M. Zuo, 2007, Phys. Rev. Lett. **99**, 196404.
Son, J., P. Moetakef, J. M. Lebeau, D. Ouellette, L. Balents, S. J. Allen, and S. Stemmer, 2010, Appl. Phys. Lett. **96**, 062114.
Stahn, J., *et al.*, 2005, Phys. Rev. B **71**, 140509.
Takahashi, K. S., M. Kawasaki, and Y. Tokura, 2001, Appl. Phys. Lett. **79**, 1324.
Takizawa, M., *et al.*, 2009, Phys. Rev. Lett. **102**, 236401.
Tebano, A., *et al.*, 2008, Phys. Rev. Lett. **100**, 137401.
Tokura, Y., 2006, Rep. Prog. Phys. **69**, 797.
Tokura, Y., 2007, J. Magn. Magn. Mater. **310**, 1145.
Tokura, Y., and N. Nagaosa, 2000, Science **288**, 462.
Tokura, Y., and Y. Tomioka, 1999, J. Magn. Magn. Mater. **200**, 1.
Tsubouchi, K., I. Ohkubo, H. Kumigashira, Y. Matsumoto, T. Ohnishi, M. Lippmaa, H. Koinuma, and M. Oshima, 2008, Appl. Phys. Lett. **92**, 262109.
Tung, I. C., P. V. Balachandran, J. Liu, B. A. Gray, E. A. Karapetrova, J. H. Lee, J. Chakhalian, M. J. Bedzyk, J. M. Rondinelli, and J. W. Freeland, 2013, Phys. Rev. B **88**, 205112.
Ueda, K., H. Tabata, and T. Kawai, 1998, Science **280**, 1064.
Velev, J. P., S. S. Jaswal, and E. Y. Tsymbal, 2011, Phil. Trans. R. Soc. A **369**, 3069.
Wang, X., M. J. Han, L. de' Medici, H. Park, C. A. Marianetti, and A. J. Millis, 2012, Phys. Rev. B **86**, 195136.
Warusawithana, M. P., E. V. Colla, J. N. Eckstein, and M. B. Weissman, 2003, Phys. Rev. Lett. **90**, 036802.
Wen, H., *et al.*, 2013, Phys. Rev. Lett. **110**, 037601.
Wu, M., *et al.*, 2013, Phys. Rev. B **88**, 125124.
Wu, S. M., S. A. Cybart, P. Yu, M. D. Rossell, J. X. Zhang, R. Ramesh, and R. C. Dynes, 2010, Nat. Mater. **9**, 756.
Xiao, D., W. Zhu, Y. Ran, N. Nagaosa, and S. Okamoto, 2011, Nat. Commun. **2**, 596.
Xie, Y., M. D. Scafetta, R. J. Sichel-Tissot, E. J. Moon, R. C. Devlin, H. Wu, A. L. Krick, and S. J. May, 2014, Adv. Mater. **26**, 1434.
Yajima, T., Y. Hikita, and H. Y. Hwang, 2011, Nat. Mater. **10**, 198.
Yang, K.-Y., W. Zhu, D. Xiao, S. Okamoto, Z. Wang, and Y. Ran, 2011, Phys. Rev. B **84**, 201104.
Yordanov, P., A. Boris, J. Freeland, J. Kavich, J. Chakhalian, H. Lee, and B. Keimer, 2011, Phys. Rev. B **84**, 045108.
Yoshimatsu, K., K. Horiba, H. Kumigashira, T. Yoshida, A. Fujimori, and M. Oshima, 2011, Science **333**, 319.
Zaanen, J., G. Sawatzky, and J. Allen, 1985, Phys. Rev. Lett. **55**, 418.
Zhang, J., and R. D. Averitt, 2014, Annu. Rev. Mater. Res. **44**, 19.
Zhang, Z. L., U. Kaiser, S. Soltan, H.-U. Habermeier, and B. Keimer, 2009, Appl. Phys. Lett. **95**, 242505.
Zhong, Z., P. X. Xu, and P. J. Kelly, 2010, Phys. Rev. B **82**, 165127.
Zubko, P., S. Gariglio, M. Gabay, P. Ghosez, and J.-M. Triscone, 2011, Annu. Rev. Condens. Matter Phys. **2**, 141.